Journal of Applied Mechanics and Technical Physics, Vol. 51, No. 4, pp. 579–589, 2010

MODELING OF FORMING OF WING PANELS OF THE SSJ-100 AIRCRAFT

B. D. Annin,[1] A. I. Oleinikov,[2,3] and K. S. Bormotin[3]

UDC 539.3

Problems of inelastic straining of three-dimensional bodies with large displacements and turns are considered. In addition to the sought fields, surface forces and boundary displacements have also to be determined in these problems. Experimental justification is given to the proposed constitutive equations of steady creep for transversely isotropic materials with different characteristics under tension and compression. Algorithms and results of the finite-element solution of the problem are presented for these materials.

Key words: *boundary conditions, inelasticity, relaxation, residual displacements.*

Introduction. In solving problems of inelastic straining with boundary conditions determined from specified residual displacements, much attention has been paid recently to the development of formulations of various classes of such problems, establishment of sufficient conditions for their correctness, and justification of iterative and step-by-step methods of solving these problems [1–5]. Application of these methods allows finding solutions for plates and rods [6–8]. A solution for a three-dimensional isotropic body was given in [9].

In practice, solving problems of this kind is usually based on using simple semi-empirical relations obtained from the analysis of an array of test solutions resulting from experiments. This approach involves considerable material and time costs, which often make the solution non-beneficial. Therefore, advanced design methods imply the search for test solutions through computer modeling of the boundary actions and straining processes [10].

1. Constitutive Relations. Based on experimental data [11–14], we use the following models of blank material straining.

Let σ_{ij} and ε_{ij} be the components of the stress and strain tensors in a rectangular Cartesian coordinate system (x_1, x_2, x_3) and let s_{ij} and e_{ij} be their deviators: $s_{ij} = \sigma_{ij} - \sigma_{pq}\delta_{pq}/3$ and $e_{ij} = \varepsilon_{ij} - \varepsilon_{pq}\delta_{pq}/3$ ($\delta_{ij} = 1$ at $i = j$ and $\delta_{ij} = 0$ at $i \neq j$). Hereinafter, summation is performed over the repeated subscripts from 1 to 3. The total strain ε_{ij} is the sum of elastic and inelastic strains:

$$\varepsilon_{ij} = \varepsilon^e_{ij} + \varepsilon^n_{ij}.$$

For inelastic strains, the incompressibility condition is valid:

$$\varepsilon^n_{ij}\delta_{ij} = 0.$$

Elastic strains are related to stresses via Hooke's law

$$\varepsilon^e_{ij} = [(1+\nu)\sigma_{ij} - \nu\delta_{ij}\sigma_{kl}\delta_{kl}]/E, \tag{1.1}$$

where E is Young's modulus and ν is Poisson's ratio.

The inelastic strain is the sum of plastic strains and creep strains:

$$\varepsilon^n_{ij} = \varepsilon^p_{ij} + \varepsilon^c_{ij}.$$

[1]Lavrent'ev Institute of Hydrodynamics, Siberian Division, Russian Academy of Sciences, Novosibirsk 630090; annin@hydro.nsc.ru. [2]Institute of Machine Science and Metallurgy, Far-East Division, Russian Academy of Sciences, Komsomol'sk-on-Amur 681005. [3]Komsomol'sk-on-Amur State Technical University, Komsomol'sk-on-Amur 681013; cvmi@knastu.ru. Translated from Prikladnaya Mekhanika i Tekhnicheskaya Fizika, Vol. 51, No. 4, pp. 155–165, July–August, 2010. Original article submitted January 25, 2010.

The criterion of reaching the initial plastic state is the Huber–Mises condition

$$(3/2)s_{ij}s_{ij} = \sigma_y^2, \tag{1.2}$$

where σ_y is the yield stress of the blank material under uniaxial tension.

The loading surface corresponds to isotropic hardening of the material:

$$f \equiv 3J_2^s - \sigma_{y*}^2 = 0.$$

Here, J_2^s is the second invariant of the deviator and σ_{y*} is the current value of the yield stress. If $f < 0$ or $f = 0$ and $(\partial f/\partial\sigma_{kl})\,d\sigma_{kl} \le 0$, then $d\varepsilon_{ij}^p = 0$. If $f = 0$ and $(\partial f/\partial\sigma_{kl})\,d\sigma_{kl} > 0$, then the plastic strain increments are written in the form

$$d\varepsilon_{ij}^p = s_{ij}h(J_2^s)\,dJ_2^s, \tag{1.3}$$

where

$$h(J_2^s) = \frac{1}{2\sqrt{6J_2^s}}\Big(\frac{1}{E_t} - \frac{1}{\mu}\Big), \qquad \mu = \frac{E}{2(1+\nu)}, \tag{1.4}$$

and E_t is the tangent modulus. For the materials considered in this paper, E_t is a constant quantity characterizing the linear hardening intensity. The creep strain increments are found by the formula

$$d\varepsilon_{ij}^c = \dot\varepsilon_{ij}^c\,dt,$$

where t is the time and $\dot\varepsilon_{ij}^c$ is the steady creep strain rate for a transversely isotropic material with the isotropy plane (x_1, x_2) and with different characteristics under tension and compression [15–18]:

$$\dot\varepsilon_{ij}^c = \gamma(\sigma_{c1}, \sigma_{c2}, \xi, \eta)s_{ij}, \qquad \gamma = f_1(\xi,\eta)\sigma_{c1}^{n_1-1} + f_2(\xi,\eta)\sigma_{c2}^{n_2-1}. \tag{1.5}$$

In the right side of Eq. (1.5), we have

$$\sigma_{cm} = \sqrt{3T_m/2}, \qquad T_m = a_mJ_1^2 + b_mJ_2 + c_mJ_3, \quad m = 1,2 \quad (a_m > 0, \quad b_m > 0, \quad c_m > 0),$$

$$\xi = J_1/\sqrt{J}, \qquad \eta = \sqrt{J_3/J}, \qquad J = J_1^2 + J_2 + J_3, \tag{1.6}$$

$$J_1 = \sigma_{33} - (\sigma_{11} + \sigma_{22})/2, \qquad J_2 = (\sigma_{11} - \sigma_{22})^2 + 4\sigma_{12}^2, \qquad J_3 = \sigma_{13}^2 + \sigma_{23}^2,$$

$$f_1(\xi,\eta) = \sum_{k=1}^{3}\prod_{\substack{l=1\\ l\ne k}}^{6}\frac{\boldsymbol{r}_l\cdot\boldsymbol{r}_{kl}}{\boldsymbol{r}_{kl}\cdot\boldsymbol{r}_{kl}}, \qquad f_2(\xi,\eta) = \sum_{k=4}^{6}\prod_{\substack{l=1\\ l\ne k}}^{6}\frac{\boldsymbol{r}_l\cdot\boldsymbol{r}_{kl}}{\boldsymbol{r}_{kl}\cdot\boldsymbol{r}_{kl}},$$

$$\boldsymbol{r}_l = (\xi - \xi_l)\boldsymbol{e}_1 + (\eta - \eta_l)\boldsymbol{e}_2, \qquad \boldsymbol{r}_{kl} = (\xi_k - \xi_l)\boldsymbol{e}_1 + (\eta_k - \eta_l)\boldsymbol{e}_2 \qquad (\boldsymbol{e}_\alpha\cdot\boldsymbol{e}_\beta = \delta_{\alpha\beta}).$$

In accordance with Eqs. (1.6), the parameters $|\xi| \le 1$ and $0 \le \eta \le 1$ determine the stress state type for the transversely isotropic body in a given direction. The constants a_m, b_m, and c_m are found from the characteristics of the steady creep segment of the creep curves obtained under pure tension ($m = 1$) and under pure compression ($m = 2$) in this direction:

$$a_1 = \frac{2}{3}\Big(\frac{3}{2}\,B_{13}\Big)^{2/(n_1-1)}, \quad b_1 = \frac{2}{3}\Big(\frac{3}{2}\,B_{11}\Big)^{2/(n_1-1)} - \frac{a_1}{4}, \quad c_1 = 4\Big(\frac{3}{2}\,B_{1\times}\Big)^{2/(n_1-1)} - \frac{a_1}{4} - b_1,$$

$$a_2 = \frac{2}{3}\Big(\frac{3}{2}\,B_{23}\Big)^{2/(n_2-1)}, \quad b_2 = \frac{2}{3}\Big(\frac{3}{2}\,B_{21}\Big)^{2/(n_2-1)} - \frac{a_2}{4}, \quad c_2 = 4\Big(\frac{3}{2}\,B_{2\times}\Big)^{2/(n_2-1)} - \frac{a_2}{4} - b_2. \tag{1.7}$$

Here, B_{13}, B_{11}, $B_{1\times}$, and n_1 are the coefficients and the power index in the dependence of the creep rate on stress under pure tension in three directions: along the x_3 and x_1 (or x_2) axes and at an angle of 45° to the x_3 axis in the plane (x_2, x_3). These tension directions are characterized by the corresponding values of the parameters ξ and η, namely, $(\xi_1,\eta_1) = (1,0)$, $(\xi_2,\eta_2) = (-1/\sqrt{5},0)$, and $(\xi_3,\eta_3) = (1/3, 2/3)$. The coefficients B_{23}, B_{21}, and $B_{2\times}$ and the power index n_2 correspond to pure compression in these directions, and $(\xi_4,\eta_4) = (-1,0)$, $(\xi_5,\eta_5) = (1/\sqrt{5},0)$, and $(\xi_6,\eta_6) = (-1/3, 2/3)$. These six points (ξ_l,η_l) are nodes of interpolation of the polynomials $f_1(\xi,\eta)$ and $f_2(\xi,\eta)$ in Eq. (1.5).

2. Numerical Methods of Solving Plasticity and Steady Creep Problems. The forming process considered includes two stages: active stage of elastoviscoplastic straining of the blank in the die tooling and passive stage of unloading of the blank withdrawn from the die tooling. The final stress-strain state at the active stage is the initial state for the passive stage. The blank is fixed to avoid its motion as a whole at both stages in an identical manner; the body and accelerative forces are ignored.

Unloading is considered as purely elastic straining, with no increments of inelastic strains. The active stage, in turn, also includes two steps. At the first step, the frontal faces of the "cold" (temperature of about 20°C) blank are pressed to the working surfaces of the die tooling, which results in elastoplastic straining of the blank. The second step includes the processes of stress relaxation and creep strain in the blank fixed in this die tooling during a given time at an elevated temperature (close to the artificial ageing temperature). The processes of blank and die tooling heating and cooling are not considered in this paper, because they are assumed to exert a minor effect on the panel forming result.

As the forming process considered mainly means bending of a comparatively thin blank, the strains are assumed to be small, while the displacements and turns are fairly large; the reference configuration in which the coordinate system (x_1, x_2, x_3) is introduced coincides with the initial configuration of the body. Thus, σ_{ij} are the components of the second Piola–Kirchhoff stress tensor and ε_{ij} are the components of the Green–Lagrange strain tensor.

The equilibrium equations are written in a weak form as

$$\int\limits_V \sigma_{ij}\,\delta\varepsilon_{ij}\,dV = \int\limits_V \rho f_i\,\delta u_i\,dV + \int\limits_{S_T} \tilde{T}_i\,\delta u_i\,dS. \tag{2.1}$$

Here, u_i and $\tilde{T}_i$ are the components of the displacement vectors and surface forces, respectively, ρ is the mass density of the blank material in the reference configuration, V is the area occupied by the body in the reference configuration, and $S = S_u \cup S_T$ ($S_u \cap S_T = \varnothing$) is the body surface; the symbol δ means the variation ($\delta u_i = 0$ on S_u).

At the active stage, the body on some part of its surface S_T is subjected to the action of the surface forces $\tilde{T}_i$

$$\tilde{T}_i = n_j\Big(\sigma_{ij} + \sigma_{jk}\,\frac{\partial u_i}{\partial x_k}\Big), \tag{2.2}$$

where n_i are the components of the unit vector of the external normal to the surface S_T in the reference configuration.

The components of the displacement vector $\tilde{u}_i$ are assigned on the part of the body surface S_u:

$$u_i = \tilde{u}_i. \tag{2.3}$$

The equations that describe the relations between the total strain tensor components ε_{ij} and the gradient of displacements $\partial u_i/\partial x_k$ have the following form:

$$\varepsilon_{ij} = \frac{1}{2}\Big(\frac{\partial u_i}{\partial x_j} + \frac{\partial u_j}{\partial x_i} + \frac{\partial u_k}{\partial x_i}\,\frac{\partial u_k}{\partial x_j}\Big). \tag{2.4}$$

Equations (2.1) are integrated step by step. Assuming the step Δt to be rather small and following [19], we obtain a linearized equilibrium equation (2.1) written in displacements:

$$\int\limits_V \delta\varepsilon : C(t) : \Delta\varepsilon\,dV + \int\limits_V \sigma(t) : \delta[\nabla\hat{\boldsymbol{u}}\cdot\nabla\hat{\boldsymbol{u}}^{\mathrm{t}}]\,dV = \int\limits_V \rho(t+\Delta t)\boldsymbol{f}(t+\Delta t)\cdot\delta\hat{\boldsymbol{u}}\,dV$$

$$+\int\limits_{S_T} \tilde{\boldsymbol{T}}(t+\Delta t)\cdot\delta\hat{\boldsymbol{u}}\,dS - \int\limits_V (\sigma(t) + \varphi(t)\,\Delta t) : \delta\varepsilon\,dV \qquad \forall\ \delta\hat{\boldsymbol{u}} \quad (\delta\hat{\boldsymbol{u}} = 0 \quad \text{on} \quad S_u). \tag{2.5}$$

Here, $\sigma = (\sigma_{ij})$, $\varepsilon = (\varepsilon_{ij})$, $\boldsymbol{u} = (u_i)$, $\hat{\boldsymbol{u}} = \Delta\boldsymbol{u}$, $\varphi = -C : (d\varepsilon^c/dt)$, the colon and the dot between the tensors indicate the operation of convolution over two and one index, respectively, ∇ is the nabla operator determined with respect to the initial configuration of the body [19], the superscript "t" means the transposition operation,

$$\Delta\varepsilon \equiv (\nabla\hat{\boldsymbol{u}} + \nabla\hat{\boldsymbol{u}}^{\mathrm{t}} + \nabla\boldsymbol{u}(t)\cdot\nabla\hat{\boldsymbol{u}}^{\mathrm{t}} + \nabla\hat{\boldsymbol{u}}\cdot\nabla\boldsymbol{u}^{\mathrm{t}}(t))/2,$$

$$C = (C_{ijkl}), \qquad C_{ijkl} = \frac{E}{1+\nu}\Big(\frac{1}{2}\,(\delta_{ik}\delta_{jl} + \delta_{il}\delta_{jk}) + \frac{1}{1-2\nu}\,\delta_{ij}\delta_{kl} - \beta\,\frac{s_{ij}s_{kl}}{1+\nu+2\alpha(J_2^s)}\Big),$$

$$\beta = \begin{cases} 0, & f < 0, \quad f = 0, \quad s_{ij}^p\, d\varepsilon_{ij} < 0, \\ 1, & f = 0, \quad s_{ij}^p\, d\varepsilon_{ij} > 0, \end{cases} \qquad \alpha(J_2^s) \equiv \frac{3}{4J_2^s}\Big(\frac{E}{E_t} - 1\Big).$$

A discrete analog of Eq. (2.5) obtained by the finite element method and by virtue of arbitrariness of the vector of increments of nodal displacements is equivalent to the following vector equation [19]:

$$K(t)\,\Delta\boldsymbol{U} = \boldsymbol{R}(t + \Delta t) - \boldsymbol{F}(t). \tag{2.6}$$

Here $\Delta\boldsymbol{U}$ is the vector of increments of nodal displacements, $\boldsymbol{R}(t + \Delta t)$ and $\boldsymbol{F}(t)$ are the vectors of external and internal forces determined at the times $t + \Delta t$ and t, respectively, and $K(t)$ is the symmetric matrix of tangent stiffness determined at the time t.

Determining the vector of increments of nodal displacements $\Delta\boldsymbol{U}$ from the system of linear equations (2.6), we can find the solution $\Delta\boldsymbol{U}(t + \Delta t)$ by the formula

$$\Delta\boldsymbol{U}(t + \Delta t) = \boldsymbol{U}(t) + \Delta\boldsymbol{U}.$$

This solution is updated by the Newton–Raphson method until the Euclidean norm of the residue vector $\boldsymbol{R}(t + \Delta t) - \boldsymbol{F}^{(k)}(t + \Delta t)$ and $\boldsymbol{U}(t + \Delta t) - \boldsymbol{U}^{(k)}(t + \Delta t)$ at the kth iteration becomes smaller than a prescribed error value.

3. Verification of Constitutive Relations of Steady Creep for Transversely Isotropic Materials with Different Properties Under Tension and Compression. The constants a_m, b_m, and c_m in Eqs. (1.5) and (1.6) are determined with the use of Eq. (1.7) from experimental curves of creep under tension and compression. For instance, for a plate made of the AK4-1T alloy [12–14], we have

$$\begin{aligned} &B_{13} = 1.6 \cdot 10^{-18}\ (\mathrm{kg/mm^2})^{-n_1} \cdot \mathrm{h}^{-1}, \qquad B_{11} = 1.2 \cdot 10^{-18}\ (\mathrm{kg/mm^2})^{-n_1} \cdot \mathrm{h}^{-1}, \\ &B_{1\times} = 3.2 \cdot 10^{-18}\ (\mathrm{kg/mm^2})^{-n_1} \cdot \mathrm{h}^{-1}, \qquad B_{23} = 4.78 \cdot 10^{-19}\ (\mathrm{kg/mm^2})^{-n_2} \cdot \mathrm{h}^{-1}, \\ &B_{21} = 5.2 \cdot 10^{-19}\ (\mathrm{kg/mm^2})^{-n_2} \cdot \mathrm{h}^{-1}, \qquad B_{2\times} = 6.6 \cdot 10^{-19}\ (\mathrm{kg/mm^2})^{-n_2} \cdot \mathrm{h}^{-1}. \end{aligned} \tag{3.1}$$

Young's modulus is $E = 6322$ kg/mm^2, $n_1 = 11$, $n_2 = 11$, and Poisson's ratio is $\nu = 0.4$.

The creep curves calculated by Eqs. (2.5), (2.6), (1.1), (1.5), and (3.1) for different constant values of tensile and compressive stresses for the same directions of the plate as those in the steady creep experiments (1.7) are in reasonable agreement with the experimental curves [17].

For comparison, we give the numerical and experimental data [12–14], which differ from the results obtained in the steady creep experiments. Figure 1 shows the calculated and experimental creep curves for pure torsion of a thin-walled sample tube whose centerline coincides with the transverse isotropy axis of the AK4-1T alloy in the plate at a temperature of 200°C.

The following geometric parameters of the tube are used in the calculations: length 10 mm; inner and outer diameters 1.84 and 2 mm, respectively; one of the tube ends is rigidly fixed, while the other end is subjected to shear forces below the yield stress. The forces are applied rather rapidly, as compared with the time during which stress relaxation occurs and creep strains are developed, but rather slowly, as compared with the time of pulsed application where accelerative effects should be taken into account. Therefore, the configuration at the initial time ($t = 0$) with zero creep strains in the numerical solution is the deformed configuration of the tube made from this elastic material under the action of constant shear forces [20]. The behavior of the sample material at the stage of force application is isotropically elastic [12–14] and is described by Hooke's law (1.1); the creep of this material is transversely isotropic with different characteristics under tension and compression and is described by the flow law (1.5).

The uniform finite element grid consists of three-dimensional hexagonal eight-node elements with the rib length of 0.196 mm. This grid interpolates the cylinder geometry and displacements by trilinear polynomials. The relative errors of the solution of Eq. (2.6) for displacements and forces are $\varepsilon_D = \varepsilon_F = 0.001$. The solution is refined at each time step by the Newton–Raphson method. The equations are integrated with an adaptive time step in the interval from 0.001 to 5 h. This is sufficient to ensure the accuracy and stability of integration of the creep strain tensor components.

It follows from Fig. 1 that the results calculated by Eqs. (1.5) ensure reasonable agreement with experimental data under pure torsion, especially under moderate stresses when the steady creep phase is realized.

For the same material, we also compare the calculated and experimental curves of deflection of a square thick-walled plate with the creep process (the transverse isotropy plane of the material is parallel to the mid-surface) under the action of four vertical concentrated forces $P = 1850$ kgf applied at the centers of the corner areas

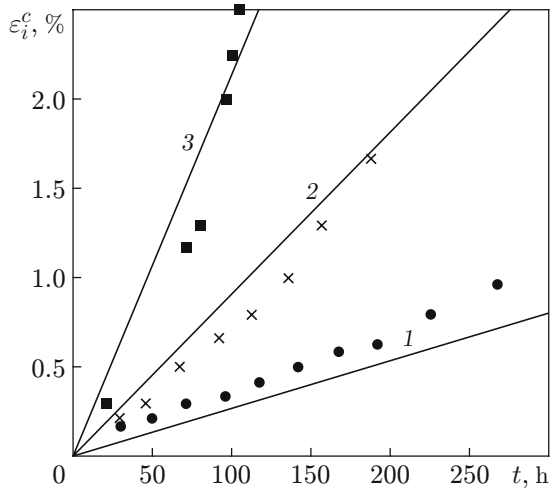

Fig. 1

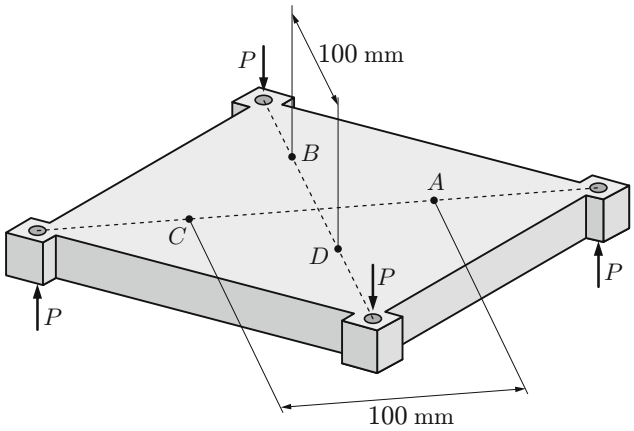

Fig. 2

Fig. 1. Calculated data (curves) and experimental data (points) on creep of the AK4-1T alloy at a temperature of 200°C under conditions of torsion of a thin-walled cylindrical sample whose centerline coincides with the transverse isotropy axis ($\sigma_i = \sqrt{3 s_{ij} s_{ij}/2}$ and $\varepsilon_i^c = \sqrt{2 \varepsilon_{ij}^c \varepsilon_{ij}^c / 3}$): $\sigma_i = 144.4$ (1), 153 (2), and 170 MPa (3).

Fig. 2. Scheme of plate loading and points A, B, C, and D where the deflection w was measured in experiments.

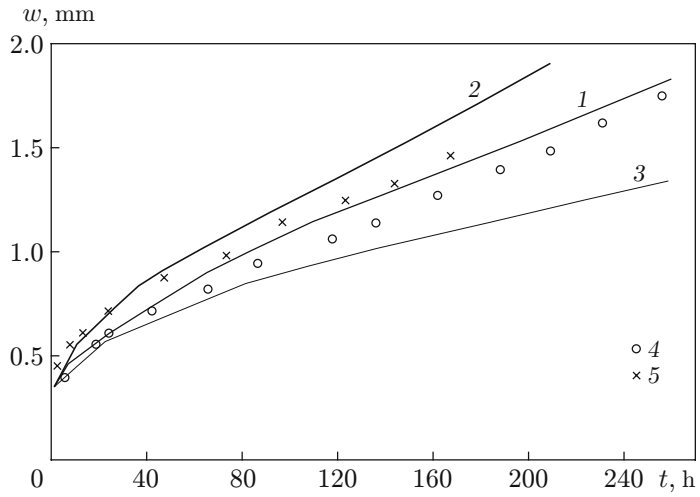

Fig. 3. Deflection at the point A of the plate versus time during the creep process under bending by the moments of torsion: curves are the results calculated with the use of constants (1.7) at a_1, b_1, c_1 and a_2, b_2, c_2 corresponding to tensile and compressive loading, respectively (curve 1), at $a_1 = a_2$, $b_1 = b_2$, and $c_1 = c_2$ corresponding to tensile loading (curve 2), and at $a_2 = a_1$, $b_2 = b_1$, and $c_2 = c_1$ corresponding to compressive loading (curve 3); points are the experimental data from experiment No. 1 (points 4) and No. 2 (points 5).

[21] (Fig. 2). The applied forces simulate pure bending of the plate by the moments of torsion with intensity $P/2$ uniformly distributed over the edges [22]. The concentrated forces were replaced in the calculations by statically equivalent loads uniformly distributed over the corner areas [20].

The points in Fig. 3 show the deflections obtained in the experiments with two identical plates (the deflections were measured at the points A, B, C, and D shown in Fig. 2 and then averaged over the four points). Figure 3 also shows the time evolution of the deflection w at the point A, which was calculated on a uniform grid consisting of three-dimensional eight-node hexagonal elements with the rib length of 10 mm.

The following geometric parameters of the plate are specified in the calculations: length 180 mm, thickness 20 mm, and corner area size 20×20. An adaptive time step in the interval from 1 to 100 h and also the same methods and criteria of solution convergence as in the previous problem on tube torsion are used.

It follows from Fig. 3 that the results calculated by Eqs. (1.5), which take into account the difference in material characteristics under tension and compression in the indicated directions (1.7), are in reasonable agreement with the results of experiments on pure bending of the plate by the moments of torsion. At the same time, it is obvious that significant errors are obtained if this difference is ignored: the calculated plate deflection is overpredicted (as compared with the experimental data) if the characteristics under tension are used in all directions and underpredicted if the characteristics under compression are used. This type of plate bending can be accurately described by the constitutive relations derived in this paper for transversely isotropic materials with different characteristics under tension and compression.

4. Problem of Wing Panel Forming. In this type of forming, the blank is also subjected to bending. In contrast to the direct problems discussed above, however, the values of the surface forces $\tilde{T}_i$ in Eq. (2.2) and boundary displacements $\tilde{u}_i$ in Eq. (2.3) are unknown in the general case and have to be determined alongside with the fields of stresses, strains, and displacements. For this purpose, it is possible to use the residual boundary displacements $\tilde{u}'_i$, for instance, the displacements $\tilde{u}'_n$ over the normal to the frontal face of the blank, which can be easily calculated from the specified geometric parameters of the panel.

Let us consider a case with the problem of forming at the stage of active loading being solved in the kinematic formulation. In this case, we have $S = S_u$, and only the boundary displacements have to be determined. We introduce an operator Ψ, which involves the displacements $\tilde{u}$ in Eq. (2.3) and relations (1.1)–(1.5), (2.1), and (2.3)–(2.6) to determine the residual boundary displacements $\tilde{u}'$:

$$\Psi\tilde{u} = \tilde{u}'.$$

Let us assume that the sought value of $\tilde{u}$ can be determined by the following iterative procedure:

$$\tilde{u}_{i+1} = \tilde{u}_i + k_i(\Psi\tilde{u}_i - \tilde{u}'), \quad i = 1, 2, \ldots, \qquad \tilde{u}_1 = \tilde{u}'. \tag{4.1}$$

The step at the $(i+1)$th iteration is increased by setting the coefficient k_i in Eq. (4.1) greater than unity; the step is reduced by setting $0 < k_i < 1$. The criterion of termination (convergence) of the iterative process (4.1) is a prescribed, rather small deviation r of the calculated residual displacements from those specified in advance:

$$H_i \equiv \|\Psi\tilde{u}_i - \tilde{u}'\| < r. \tag{4.2}$$

Figure 4 shows the error of the quantity u_{yi} in the homogeneous ($[H_{yi} = \max\limits_{S_a} |\Psi\tilde{u}_{yi} - \tilde{u}'_y|$) and root-mean-square $\left[H_{yi} = \left(\sum\limits_{S_a} (\Psi\tilde{u}_{yi} - \tilde{u}'_y)^2\right)^{1/2}\right]$ metrics at $k_i = 1$ in Eq. (4.1) (S_a is the aerodynamic surface of the panel). The curves in Fig. 4 are obtained by calculating the forming of one wing panel of the "Sukhoi SuperJet-100" (SSJ-100) airplane. It is seen from Fig. 4 that the iterative process (4.1) of determining the boundary displacements converges.

The calculation scheme with attachment conditions is shown in Fig. 5.

The blank has an irregular contour and thickness; the length varies from 13,000 to 13,500 mm; the width varies from 250 to 1600 mm; the thickness varies from 2.5 to 10.0 mm; the outer frontal face is smooth; the inner face is irregularly engraved and has longitudinal and transverse stiffeners, as well as local and contour thinning and thickening places. The blank has the following mechanical characteristics: at $T = 20°\text{C}$, Young's modulus $E = 6027$ kg/mm^2, Poisson's ratio $\nu = 0.345$, yield stress $\sigma_{\text{yield}} = 43$ kg/mm^2, and linear hardening modulus $E_{\text{yield}} = 282.4$ kg/mm^2; at $T = 180°\text{C}$, $E = 6027$ kg/mm^2 and $\nu = 0.345$; creep characteristics under tension $B_1 = 4.05 \cdot 10^{-35}$ (kg/mm^2)$^{-n_1} \cdot$ sec^{-1} and $n_1 = 20$; creep characteristics under compression $B_1 = 6.7 \cdot 10^{-29}$ (kg/mm^2)$^{-n_2} \cdot$ sec^{-1} and $n_2 = 15$.

The nonuniform finite element grid is formed from tetrahedral four-node elements with trilinear interpolation of the blank geometry and displacements. To ensure sufficient accuracy of the calculations, the distance between the nodes is taken to be approximately 2 mm; the total number of elements is 466,229. The criterion of calculation convergence is $\varepsilon_D = \varepsilon_F = 0.01$. The initial time step is 0.01.

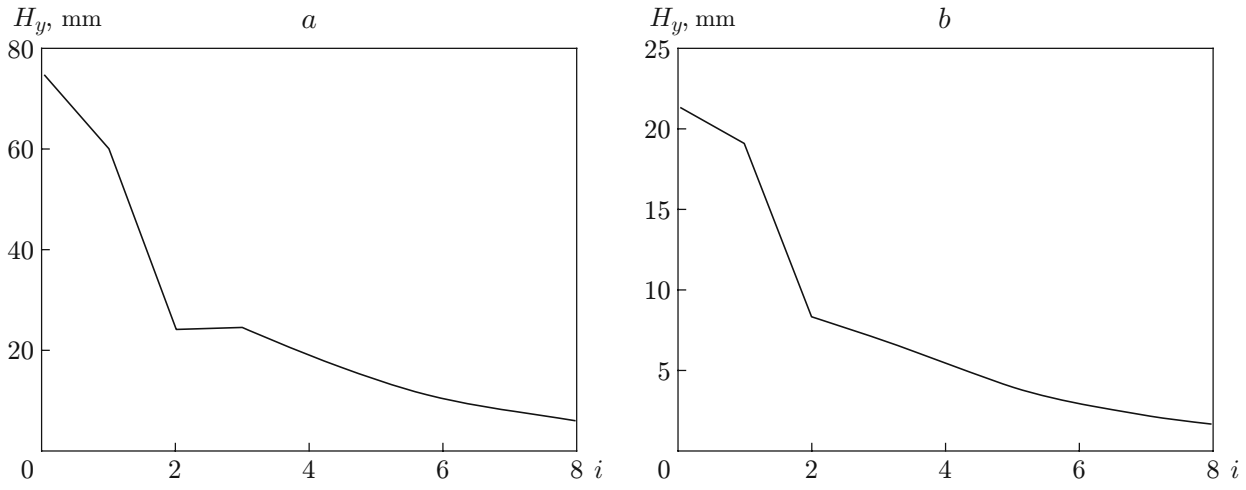

Fig. 4. Behavior of H_y (4.2) on the aerodynamic surface of the panel in the iterative process (4.1) in the homogeneous metric (a) and root-mean-square metric (b).

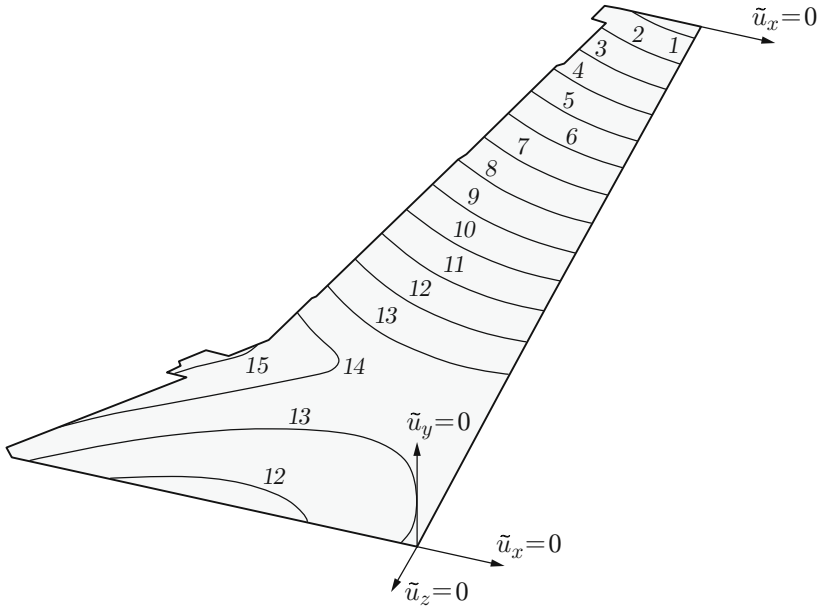

Fig. 5. Distributions of the boundary displacements $\tilde{u}_y$ calculated at the 8th iteration and attachment conditions: $\tilde{u}_y = 8.69 \cdot 10^2$ (1), $7.95 \cdot 10^2$ (2), $7.20 \cdot 10^2$ (3), $6.46 \cdot 10^2$ (4), $5.71 \cdot 10^2$ (5), $4.97 \cdot 10^2$ (6), $4.22 \cdot 10^2$ (7), $3.48 \cdot 10^2$ (8), $2.73 \cdot 10^2$ (9), $1.99 \cdot 10^2$ (10), $1.24 \cdot 10^2$ (11), 49.7 (12), -24.8 (13), -99.3 (14), and $-1.74 \cdot 10^2$ mm (15).

Using Eq. (4.1), we find the sought elements of the boundary displacements $\tilde{u}_y$ for Eq. (2.3) ($S = S_u = S_a$). The distributions of these components at the 8th iteration are shown in Fig. 5. Using these displacements, we modeled all stages of the forming process. The distributions of the intensity of the Mises shear stresses $\sigma_i = \sqrt{3 s_{ij} s_{ij}/2}$ and the strains $\varepsilon_i^c = \sqrt{2 \varepsilon_{ij}^c \varepsilon_{ij}^c / 3}$ over the outer (smooth) surface S_a and over the inner (milled and engraved) surface at certain characteristic instants of this process are shown in Figs. 6–9.

Figure 6 corresponds to the instant when the surface S_a is subjected to the displacement component $\tilde{u}_y$ (see Fig. 5). Application of these displacements simulates elastoplastic approaching of the smooth frontal surface of the "cold" (temperature approximately 20°C) blank to the die tooling working profile. Figures 7 and 8 correspond to the end of the stress relaxation period (45 min) under creeping conditions for the blank at a constant elevated

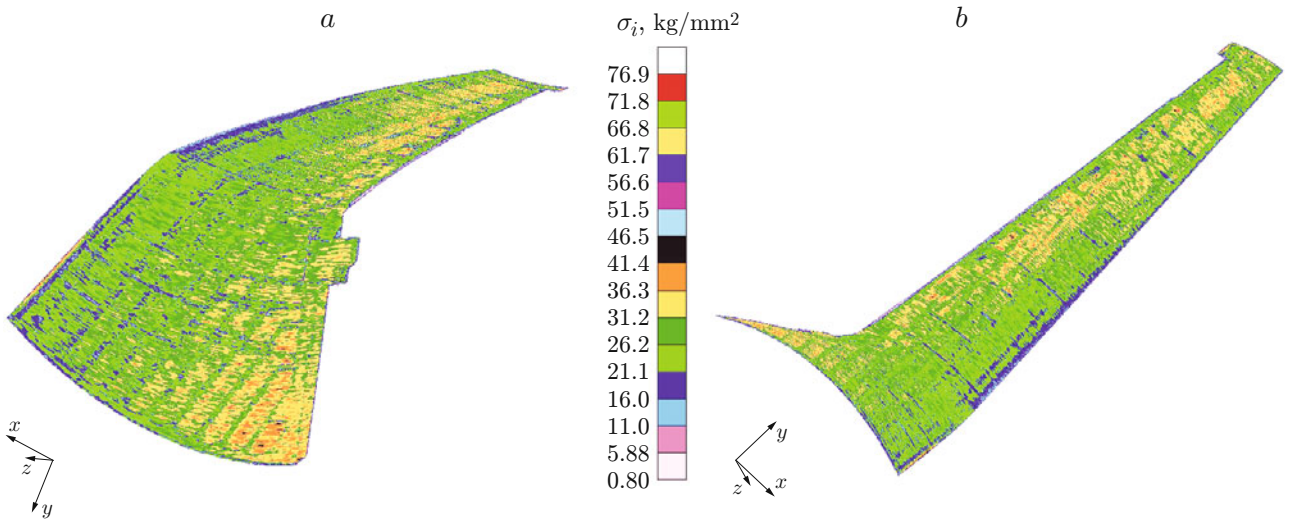

Fig. 6. Shear stress intensity distributions over the inner surface (a) and outer surface (b) of the "cold" blank in the course of approaching the die tooling working surfaces.

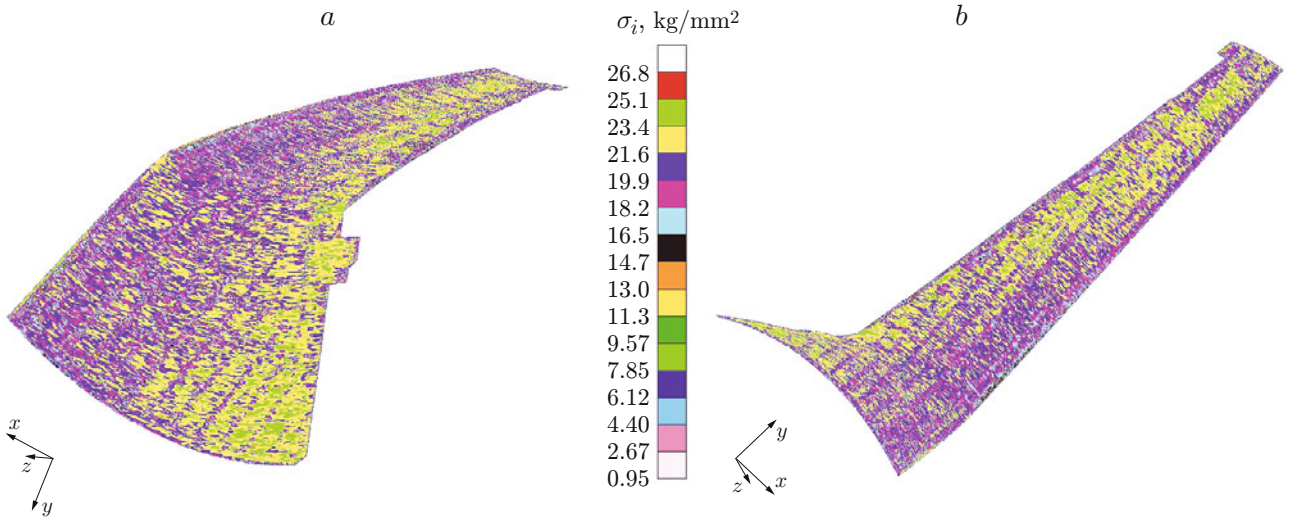

Fig. 7. Shear stress intensity distributions over the inner surface (a) and outer surface (b) of the "hot" blank after relaxation under conditions of thermal stabilization on the die tooling.

temperature ($T = 180°C$) and displacement components $\tilde{u}_y$ applied to S_a (see Fig. 5), which model thermal stabilization of the "hot" blank on the die tooling. Figure 9 shows the distribution of the residual stresses after elastic unloading of the blank from the state illustrated in Figs. 7 and 8. This unloading represents withdrawing of the cooled blank from the die tooling.

The mosaic-type character of the distributions in Figs. 6–9 is caused by the influence of the cuts in the inner panel engraving: longitudinal and transverse ribs and local thinning and thickening areas.

It follows from Fig. 6 that the yield stress excess and plastic straining are observed in small volumes on the sharp corners of the inner engraving (i.e., localization of plastic strains occurs); in the main volume, the blank approaching the die tooling proceeds in the elastic mode: the mean value of stresses is 30 kg/mm^2, and the mean value of plastic strains is 0.001.

It follows from Figs. 6a, 7, and 8a that this thermal stabilization of the hot blank on the die tooling is accompanied by stress relaxation; this relaxation is more intense in stress concentration zones; the stress field

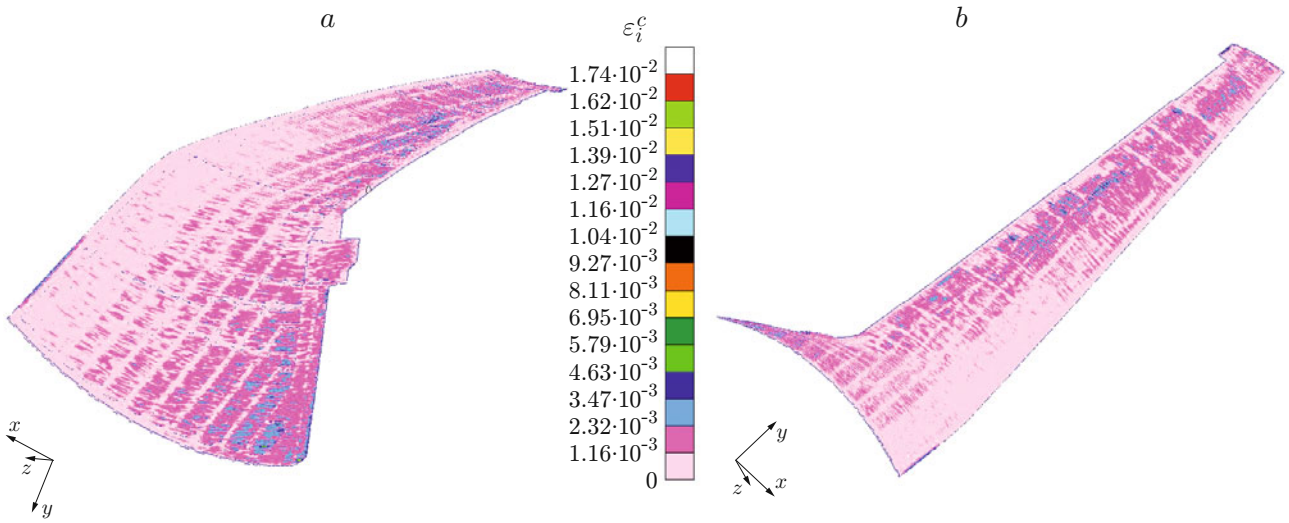

Fig. 8. Creep strain stress intensity distributions over the inner surface (a) and outer surface (b) of the "hot" blank after relaxation under conditions of thermal stabilization on the die tooling.

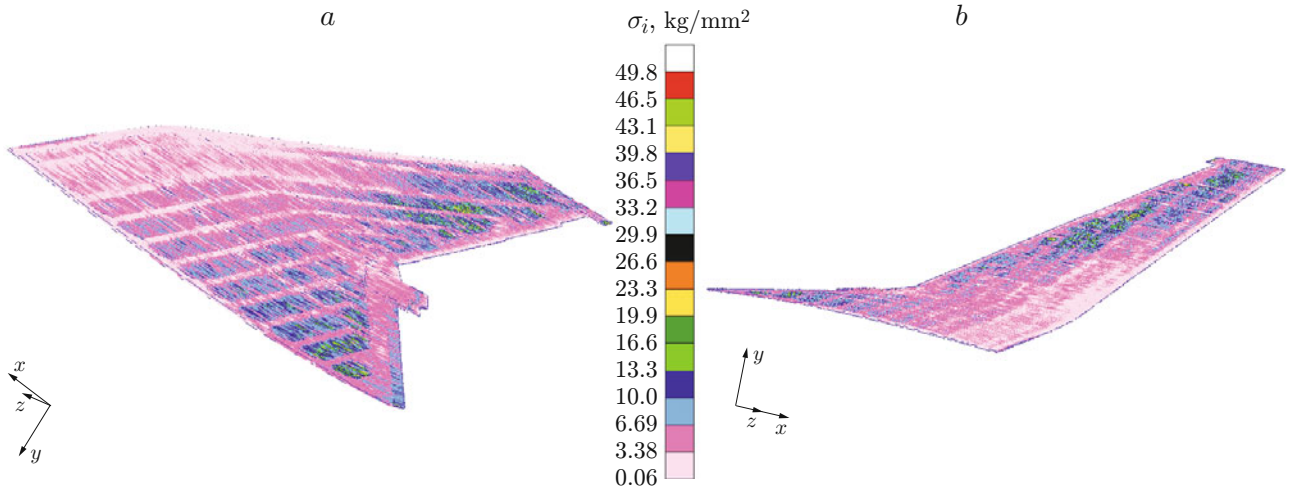

Fig. 9. Residual shear stress intensity distributions over the inner surface (a) and outer surface (b) of the panel after withdrawing of the cooled panel from the die tooling.

after relaxation becomes more uniform; the difference between the maximum and minimum stresses and also the maximum value of stresses decrease almost by a factor of 3. The relaxation is accompanied by the emergence and growth of the creep strain (see Figs. 8b and 9a); the creep strain value after relaxation reaches 17.5%. The residual stresses (see Fig. 9b) in the main volume of the formed panel reach 7 kg/mm^2.

Conclusions. The constitutive relations between the steady creep strain rates and stresses describe steady, transversely isotropic creep with different characteristics under tension and compression. Computer modeling of these forming processes involves the use of the finite element method for consecutive solutions of three-dimensional quasi-static problems of elastoplastic straining, relaxation, and unloading with allowance for large displacements and turning angles, anisotropy, and different resistances of the material, and also determining boundary conditions from given residual displacements. The proposed iterative process makes it possible to determine the sought boundary displacements. The modeling results can be used to calculate the die tooling, determine the panel processibility, and control panel rejection in the course of forming. The solution obtained is approved by special industrial tests

[10, 23]. The modeling results are used in production of integral panels at the joint-stock company "Komsomol'sk-on-Amur aircraft production association." The models and methods developed can also be used to improve the technological possibilities of production and increasing of the quality and lifetime of large contour-forming parts with new complicated aerohydrodynamic shapes, which are made of advanced high-strength light materials.

This work was supported by the Ministry of Education and Science of the Russian Federation within the Targeted Program "Development of the Scientific Potential of the Higher School (2009–2010)" (project code No. 2.1.1/1686), by the Program No. 11 of the Presidium of the Russian Academy of Sciences (project code No. 09-I-P11-03), by the Integration Project of the Siberian Division of the Russian Academy of Sciences, Ural Division of the Russian Academy of Sciences, and Far-East Division of the Russian Academy of Sciences "Modeling of Straining Processes with Allowance for Numerous Factors Affecting the Medium Behavior and External Actions," and by the Russian Foundation for Basic Research (Grant Nos. 07-01-00747 and 09-01-98514-r_vostok_a).

REFERENCES

1. I. Yu. Tsvelodub, *Stability Postulate and Its Application to the Theory of Creep of Metals* [in Russian], Inst. of Hydrodynamics, Sib. Div., Russian Acad. of Sci., Novosibirsk (1991).
2. I. Yu. Tsvelodub, "Inverse problems of inelastic straining," *Izv. Ross. Akad. Nauk, Mekh. Tverd. Tela*, No. 2, 81–92 (1995).
3. I. Yu. Tsvelodub, "Inverse problems of deformation of nonlinear viscoelastic bodies," *J. Appl. Mech. Tech. Phys.*, **38**, No. 3, 453–464 (1997).
4. I. Yu. Tsvelodub, "Inverse elastoplastic problem," *Izv. Ross. Akad. Nauk, Mekh. Tverd. Tela*, No. 1, 35–43 (1998).
5. I. V. Sukhorukov and I. Yu. Tsvelodub, "Iterative method for solving inverse relaxation problems," *Izv. Akad. Nauk SSSR, Mekh. Tverd. Tela*, No. 3, 93–101 (1991).
6. I. A. Banshchikova and I. Yu. Tsvelodub, "On one class of inverse problems of variation in shape of viscoelastic plates," *J. Appl. Mech. Tech. Phys.*, **37**, No. 6, 876–883 (1996).
7. I. A. Banshchikova, "Inverse problem for a viscoelastic plate," in: *Dynamics of Continuous Media* (collected scientific papers) [in Russian], No. 113, Inst. of Hydrodynamics, Sib. Div., Russian Acad. of Sci., Novosibirsk (1998), pp. 13–18.
8. A. I. Banshchikova, B. V. Gorev, and I. V. Sukhorukov, "Two-dimensional problems of beam forming under conditions of creep," *J. Appl. Mech. Tech. Phys.*, **43**, No. 3, 448–456 (2002).
9. A. I. Oleinikov, "Modeling of forming processes for panel of the Russian regional plane," in: *Abstracts of IX All-Russia Forum on Theoretical and Applied Mechanics* (Nizhnii Novgorod, August 22–28, 2006), Vol. 3, Nezhegor. Gos. Univ., Nizhnii Novgorod (2006), p. 162.
10. A. I. Oleinikov and A. I. Pekarsh, *Integrated Design of Integral Panel Manufacture Processes* [in Russian], Ékom, Moscow (2009).
11. B. V. Gorev, I. Zh. Masanov, A. I. Pekarsh, and A. I. Oleinikov, "Specific features of the strain and strength behavior of aluminum-based sheet materials, as applied to part forming under creeping conditions," in: *Dynamic and Process Issues in Structures and Continuum Mechanics*, Proc. 11th Int. Symp., Vol. 1, Moscow Aviation Inst., Moscow (2005), pp. 115–117.
12. B. V. Gorev and I. Zh. Masanov, "Specific features of straining of structural sheets made of aluminum alloys in the creeping mode," *Tekhnol. Mashinostr.*, No. 7, 13–20 (2009).
13. V. B. Gorev and O. V. Sosnin, "Some specific features of creep of sheeted materials," in: *Dynamics of Continuous Media* (collected scientific papers) [in Russian], No. 4, Inst. of Hydrodynamics, Sib. Div., USSR Acad. of Sci., Novosibirsk (1970), pp. 5–10.
14. V. V. Rubanov, "Experimental verification of the incompressibility hypothesis on the AK4-1T aluminum alloy," in: *Dynamics of Continuous Media* (collected scientific papers) [in Russian], No. 75, Inst. of Hydrodynamics, Sib. Div., USSR Acad. of Sci., Novosibirsk (1985), pp. pp. 126–131.
15. B. D. Annin, "Models of elastoplastic straining of transversely isotropic materials," *Sib. Zh. Industr. Mat.*, **2**, No. 2, 3–7 (1999).

16. A. I. Oleinikov, "Steady creep models for isotropic and transversely isotropic materials with different properties under tension and compression," in: *Achievements of Mechanics of Continuous Media, Abstracts of All-Russian Conf. Devoted to the 70th Anniversary of Academician V. A. Levin* [in Russian], Dal'nauka, Vladivostok (2009), p. 98.
17. A. I. Oleinikov and K. S. Bormotin, "Steady creep models for design of manufacture processes for structural elements," in: *ibid.*, pp. 571–582.
18. A. I. Oleinikov, "Steady creep models for transversely isotropic materials with different properties under tension and compression," *Sib. Zh. Industr. Mat.*, **13**, No. 3, 52–59 (2010).
19. S. N. Korobeinikov, *Nonlinear Straining of Solids* [in Russian], Izd. Sib. Otd. Ross. Akad. Nauk, Novosibirsk (2000).
20. A. I. Oleinikov, S. N. Korobeinikov, B. V. Gorev, and K. S. Bormotin, "Mathematical simulation of creeping processes for metal products made of materials with different properties in tension and compression," *Vychisl. Metody Program.*, **9**, 346–365 (2008).
21. O. V. Sosnin, B. V. Gorev, and V. V. Rubanov, "Torsion of a square plate made of a material with different resistances to tension and compression at creeping," in: *Strength Calculations of Ship Structures and Mechanisms* (collected scientific papers), [in Russian], No. 117, Institute of Water Transport Engineering, Ministry of Inland Water Transport, Novosibirsk (1976), pp. 78–88.
22. S. P. Timoshenko and S. Woinowsky-Krieger, *Theory of Plates and Shells*, McGraw-Hill, New York (1959).
23. A. I. Oleinikov, A. I. Pekarsh, V. V. Bakaev, et al., "Pre-production of complicated parts with a double variable-sign curvature by the finite element method used to analyze the geometric model with complex updating of the die tooling, part involute, and recommendations on the technological process," *SAPR Grafika*, No. 2, 88–96 (2009).